

# Heavy Alkali Treatment of Post-Sulfurized Cu(In,Ga)Se<sub>2</sub> Layers: Effect on Absorber Properties and Solar Cell Performance

Jan Keller,\* Oleksandr V. Bilousov, Janet Neerken, Erik Wallin, Natalia M. Martin, Lars Riekehr, Marika Edoff, and Charlotte Platzer-Björkman

This contribution evaluates a sequential post-deposition treatment of Cu(In,Ga)Se<sub>2</sub> (CIGS) films, consisting of 1) a post-sulfurization in elemental S-atmosphere and 2) a subsequent treatment by heavy alkali fluorides (Alk-PDT). First, the effect of the sulfurization step on the corresponding solar cell performance is investigated and optimum process parameters, leading to an efficiency improvement, are identified. Losses in carrier collection observed after S-incorporation are attributed to an increased grain boundary (GB) recombination. It is found that the corresponding reduction in short-circuit current density can be mitigated by a RbF- or KF-PDT, supposedly by depleting GBs in Cu. However, in strong contrast to non-sulfurized CIGS, the Alk-PDT results in a lower open-circuit voltage and distortions in the current–voltage (*I*–*V*) characteristics for sulfurized absorbers. Possible explanations are the absence of a wide-gap surface phase and/or air exposure between the post-treatment steps. It is further proposed that a back contact barrier may be responsible for the distortions in *I*–*V*.

bulk properties, such as the passivation of deep trap states,<sup>[5]</sup> an increased electron lifetime,<sup>[1]</sup> and an increased hole mobility,<sup>[6]</sup> are also discussed.

As the sulfur incorporation can be confined to the very surface region, the open-circuit voltage (*V*<sub>OC</sub>) can be increased without obtaining major losses in absorption and, correspondingly, in short-circuit current density (*J*<sub>SC</sub>). This makes the sulfurization step particularly interesting for CIGS bottom cells (*E*<sub>G</sub> = 1–1.1 eV) in tandem applications with, e.g., perovskite top cells.<sup>[7–10]</sup> The large potential of this cell combination was recently highlighted by a new record efficiency of 24.2% for a 2-terminal device.<sup>[11]</sup>

To combine the greater flexibility in tailoring the absorber composition (Ga/In profile) with the surface modifications by the S-treatment, a post-annealing of co-evaporated CIGS in either H<sub>2</sub>S<sup>[3,12–14]</sup> or elemental sulfur<sup>[15–19]</sup> was frequently studied. In the present contribution, the latter approach is followed, mainly to avoid usage of toxic H<sub>2</sub>S gas. Previous experiments have shown that this process results in the formation of a relatively conformal, ternary CuInS<sub>2</sub> surface layer, independent of the initial presence of Ga at the surface. However, to avoid the formation of a detrimental high-Ga phase (i.e., transport barrier) underneath the CuInS<sub>2</sub> layer during sulfurization, the initial absorber should be Ga-free at the very surface.<sup>[16,17,20]</sup> Furthermore, it was observed that the benefit of the post-sulfurization is increasing when approaching stoichiometric absorber

## 1. Introduction


Sulfur incorporation into the surface region of Cu(In,Ga)Se<sub>2</sub> (CIGS) material is commonly utilized for sequentially processed absorbers in thin film solar cells and modules.<sup>[1,2]</sup>

Replacing Se by S and thereby forming Cu(In<sub>1–*x*</sub>Ga<sub>*x*</sub>)(Se<sub>1–*y*</sub>S<sub>*y*</sub>)<sub>2</sub> increases the band gap energy (*E*<sub>G</sub>) by lowering the valence band maximum (*E*<sub>V</sub>) and, to a slightly larger extent, lifting the conduction band minimum (*E*<sub>C</sub>).<sup>[3,4]</sup> Thus, an electronic barrier for holes toward the potentially defect-rich buffer/absorber interface can be created, which reduces interface and space charge region (SCR) recombination. In addition, beneficial effects related to

Dr. J. Keller, Dr. N. M. Martin, Dr. L. Riekehr, Prof. M. Edoff,  
Prof. C. Platzer-Björkman  
Ångström Solar Center  
Division of Solar Cell Technology  
Uppsala University  
75121 Uppsala, Sweden  
E-mail: jan.keller@angstrom.uu.se

Dr. O. V. Bilousov, Dr. E. Wallin  
Solibro Research AB  
Vallvägen 5, 75151 Uppsala, Sweden

J. Neerken  
Ultrafast Nanoscale Dynamics  
Institute of Physics  
University of Oldenburg  
D-26111 Oldenburg, Germany

 The ORCID identification number(s) for the author(s) of this article can be found under <https://doi.org/10.1002/solr.202000248>.

© 2020 The Authors. Published by WILEY-VCH Verlag GmbH & Co. KGaA, Weinheim. This is an open access article under the terms of the Creative Commons Attribution License, which permits use, distribution and reproduction in any medium, provided the original work is properly cited.

DOI: 10.1002/solr.202000248

composition,<sup>[17]</sup> which is required for S-incorporation.<sup>[21]</sup> For Cu-poor absorbers, long-range diffusion, presumably via grain boundaries (GBs), is required to supply Cu to the reaction front. Indeed, Cu was found enriched in S-containing GBs after sulfurization.<sup>[20]</sup> As a result, ordered vacancy compound domains form in the bulk as well as directly underneath the CuInS<sub>2</sub>, supposedly trapping charge carriers and/or creating local transport barriers.<sup>[17]</sup> In addition to the formation of CuInS<sub>2</sub>, S is further 1) incorporated in Cu(In,Ga)(Se,S)<sub>2</sub> mixed crystals, which are spatially confined and rather randomly distributed underneath the CuInS<sub>2</sub> layer, 2) diffusing along the grain boundaries toward the back contact,<sup>[15,17,20,22]</sup> and 3) bound in plate-like Na-In-S compounds on the surface.<sup>[17]</sup> Taking all these findings into account, a CIGS film with no Ga at the front surface (about the top 500 nm are Ga-free) and close-stoichiometric composition was used as a baseline for the sulfurization experiments in this study.

In recent years, the application of a heavy alkali metal fluoride (i.e., KF, RbF, and CsF) post-deposition treatment (Alk-PDT) after CIGS absorber formation was established,<sup>[23]</sup> potentially boosting  $V_{OC}$  and/or the fill factor (FF) and allowing for a reduced CdS buffer thickness and thereby higher  $J_{SC}$ .<sup>[8,24–29]</sup> While the gain in  $J_{SC}$  is clearly explained, there is still a very controversial discussion about the origin of the  $V_{OC}$  (and FF) gain.<sup>[30,31]</sup> In most studies, a very thin, wide-gap surface phase is observed and commonly attributed to an Alk-In-Se (e.g., AlkInSe<sub>2</sub>) compound.<sup>[32–34]</sup> It is argued that this layer may act as a surface passivation and thereby increases  $V_{OC}$ . However, it is not clear if this phase always forms and if/when it occurs as a closed layer or rather as distributed clusters.<sup>[30,35]</sup> On the contrary, a suppression of bulk recombination is discussed. While a reduced concentration of deep defects by the Alk-PDT appears unlikely,<sup>[30]</sup> it was suggested that a detrimental band-bending at GBs is reduced by the introduction of heavy alkalis (expressed as reduced band-tailing), which may agglomerate in GBs as AlkInSe<sub>2</sub> and reduce/passivate charged defects.<sup>[30,36,37]</sup> The Alk-PDT further affects the apparent doping density, but opposite trends (i.e., higher and lower doping) were observed.<sup>[38–40]</sup>

Similar to pure, co-evaporated Cu(In,Ga)Se<sub>2</sub> films, it was shown that also for sulfur-containing absorbers a heavy alkali (i.e., K, Rb, and Cs) post-deposition treatment can lead to a distinct improvement in device performance, allowing for efficiencies of up to  $\eta = 23.4\%$ .<sup>[41–43]</sup> However, to the best of our knowledge, the Alk-PDT was not studied yet on co-evaporated CIGS post-sulfurized in elemental S-atmosphere. It may be expected that the pure CuInS<sub>2</sub> surface shows a different reaction behavior during Alk-PDT.

In this work, the effect of a RbF- and KF-PDT on post-sulfurized CIGS is investigated. To understand the effects on device performance, the first part elaborates the impact of the sulfurization step on the opto-electronical properties of samples without Alk-PDT. In the second part, these results will be compared with solar cells which were subjected to various doses of RbF and KF. Finally, chemical and microstructural analysis is conducted to explain the observed differences in device characteristics.

## 2. Results and Discussion

This section is separated into three paragraphs. First, the impact of the sulfurization parameters on the solar cell performance is

presented and discussed. In the second part, the effect of a subsequent KF- or RbF-PDT step is studied. Finally, the spatial incorporation of heavy alkalis in sulfurized CIGS is investigated by glow discharge-optical emission spectroscopy (GDOES) and energy-dispersive X-ray spectroscopy in scanning transmission electron microscopy (STEM-EDS). For the sake of clarity, only the current-voltage ( $I$ - $V$ ) and external quantum efficiency (EQE) results of the best solar cell (highest efficiency) of each sample are presented. The trends for average values are identical.

### 2.1. Sulfurization Parameters versus Solar Cell Performance without Alk-PDT

#### 2.1.1. $I$ - $V$ and Quantum Efficiency Analysis

Figure 1 shows the  $I$ - $V$  characteristics of solar cells without (Ref) and with a sulfurization step at different conditions (ordered by increasing S-incorporation). The corresponding solar cell parameters are shown in Table 1. Clear trends can be observed. With increasing sulfur addition,  $V_{OC}$  is increasing and  $J_{SC}$  is decreasing. While the main gain in  $V_{OC}$  results from the sulfur incorporation,<sup>[16,17]</sup> a minor additional effect of Ga diffusion toward the surface cannot be excluded for  $T_s \geq 560^\circ\text{C}$  (small Ga signal detected at the surface by GDOES [not shown here]). The FF values are increasing until a maximum of 71.2% is

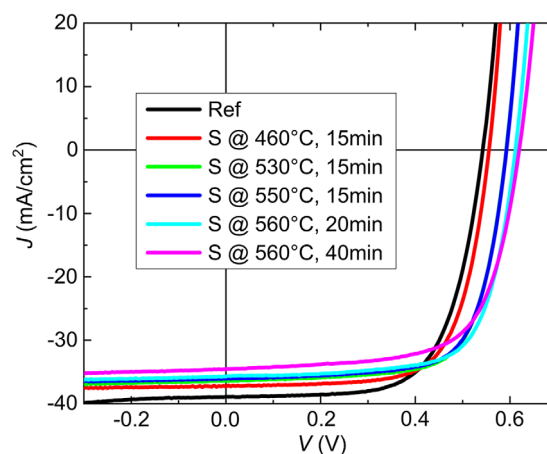


**Figure 1.**  $I$ - $V$  characteristics of the best solar cells for the reference and after sulfurization at different conditions (all without Alk-PDT).

**Table 1.** Device parameters of the best solar cells for the reference and after sulfurization at different conditions (all without Alk-PDT) as deduced from  $I$ - $V$  characterization (see Figure 1).

Sample	FF [%]	$J_{SC,EQE}$ [mA cm <sup>-2</sup> ]	$V_{OC}$ [mV]	$\eta$ [%]	$R_{SH}$ [ $\Omega$ cm <sup>2</sup> ]
Ref	66.7	38.9	542	14.1	703
S @ 460 °C	69.6	37.4	556	14.5	681
S @ 530 °C	70.9	36.5	592	15.3	486
S @ 550 °C	71.2	36.1	593	15.2	549
S @ 560 °C (20 min)	70.9	35.7	611	15.5	497
S @ 560 °C (40 min)	67.2	34.6	619	14.4	346

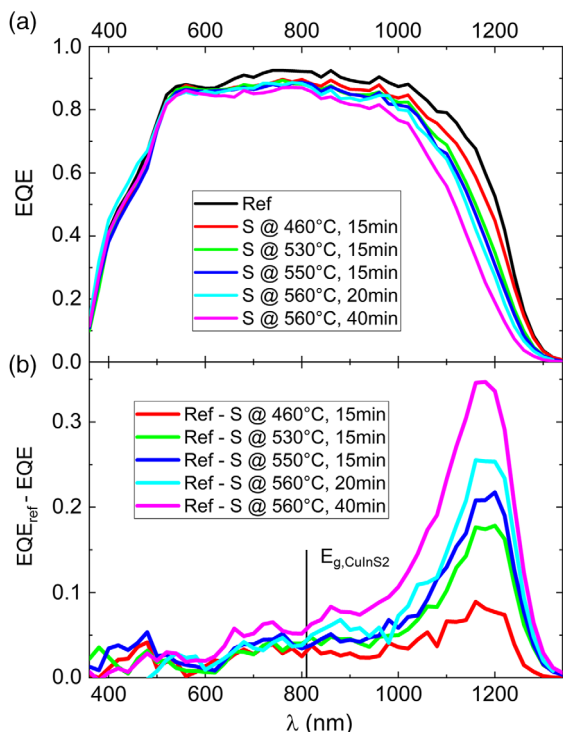


**Figure 2.** a) EQE of the best solar cells for the reference and after sulfurization at different conditions (without Alk-PDT). b) Absolute reductions in EQE after sulfurization as compared to the Ref sample.

reached for 15 min sulfurization at 550 °C. This trend is mainly ascribed to the increase in  $V_{OC}$ .<sup>[44]</sup> For a larger S-incorporation, the FF is decreasing again. The origin of this effect will be discussed later in the text. Finally, a gain in efficiency is obtained for all samples, which is largest for the sample sulfurized for 20 min at 560 °C.

The apparent shunt resistance  $R_{SH}$ , as derived from the inverse slope in the interval  $V = -0.1$  to  $+0.1$  V, is added in Table 1, too. It is obvious that  $R_{SH}$  is decreased by the sulfurization treatment. This indicates a larger voltage dependency of the photocurrent for the sulfurized solar cells because  $R_{SH}$  is similar for all samples when deduced from  $I$ - $V$  measurements in the dark (not shown here).

Figure 2a shows the measured EQE spectra used to calculate the  $J_{SC,EQE}$  values in Table 1. To understand the spectral losses in dependency of the sulfurization intensity, Figure 2b shows the absolute reductions in EQE as compared with the Ref sample. It is evident that with increasing S-introduction larger losses in  $J_{SC}$  occur, mainly for  $\lambda > 1000$  nm. In general, all solar cells lose continuously more photocurrent with increasing wavelength, starting at  $\lambda \approx 600$  nm. In the following paragraph, the origin of the observed losses in  $J_{SC}$  will be discussed. From here on we focus on the “S @ 530 °C” sample because the Alk-PDT experiments and microstructural characterization were conducted on this absorber.

### 2.1.2. Origin of Collection Losses after Sulfurization

Figure 3 shows the band diagram (electron energy related to Fermi energy  $[E_F]$ ) of a solar cell heterojunction with a

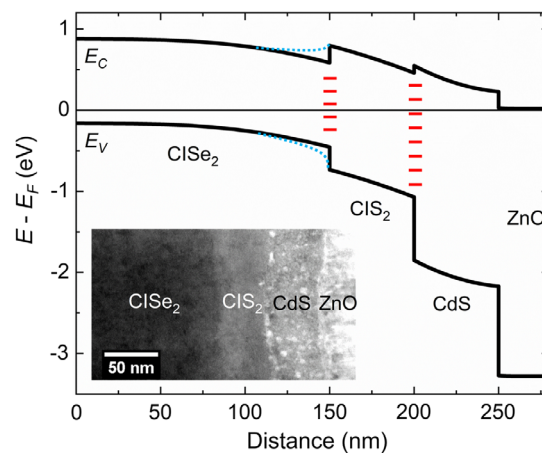


**Figure 3.** Band diagram estimated for a sample with 15 min sulfurization @ 530 °C as generated by SCAPS-1D (zoomed into heterojunction region). The dashed blue lines are added to indicate the effect of possible CuIn(S<sub>x</sub>S<sub>1-x</sub>)<sub>2</sub> regions underneath the CuInS<sub>2</sub>. The inset shows a BF-STEM image of the heterojunction of the sample sulfurized at 530 °C.

50 nm-thick CuInS<sub>2</sub> layer in-between the CuInSe<sub>2</sub> absorber and the CdS buffer layer, as computed by the solar cell device simulator SCAPS-1D.<sup>[45]</sup> The dashed blue lines sketch the effect of a possible CuIn(S<sub>x</sub>S<sub>1-x</sub>)<sub>2</sub> region underneath the CuInS<sub>2</sub> with laterally varying extension. This sequence corresponds approximately to the heterojunction of the sample subjected to a 15 min sulfurization at 530 °C, which resulted in a CuInS<sub>2</sub> layer thickness of 40–60 nm, as illustrated in the bright-field (BF) STEM image inset.

Electron affinities of  $\chi_{CdS} = 4.25$  eV,  $\chi_{CuInS_2} = 4.34$ , and  $\chi_{CuInSe_2} = 4.55$  eV are assumed according to refs. [4,46]. Thus, conduction band offsets of  $\approx 200$  and  $\approx 100$  meV are expected at the CuInSe<sub>2</sub>/CuInS<sub>2</sub> and CuInS<sub>2</sub>/CdS interfaces, respectively. Furthermore, constant doping densities in the absorber ( $N_{A,CuInS_2} = N_{A,CuInSe_2} = 4 \times 10^{16}$  cm<sup>-3</sup>) and buffer layer ( $N_{D,CdS} = 1 \times 10^{17}$  cm<sup>-3</sup>) are used. For the sake of simplicity, the effect of the diverse local formation of CuIn(S<sub>x</sub>S<sub>1-x</sub>)<sub>2</sub>-mixed crystals was neglected when generating the band diagram. The following discussion is also based on the assumption of a direct CuInSe<sub>2</sub>/CuInS<sub>2</sub> interface. This is a reasonable first approximation because a step-like decrease to very low, decaying S concentrations is observed underneath the CuInS<sub>2</sub> layer when the CuIn(S<sub>x</sub>S<sub>1-x</sub>)<sub>2</sub> patches are present.<sup>[17]</sup> The (rather weak) impact of such a low S-incorporation is mainly restricted to a slight reduction in the band offsets toward the CuInS<sub>2</sub>.

From a pure band-diagram perspective, several beneficial and detrimental impacts of the sulfurization may be discussed. First, the type inversion at the potentially defect-rich absorber/CdS interface is reduced, leading to a higher recombination probability. On the contrary, the increased  $E_C$  by the CuInS<sub>2</sub> formation and the valence band offset at the CuInSe<sub>2</sub>/CuInS<sub>2</sub> interface act as an effective transport barrier for holes toward the buffer, if generated underneath the CuInS<sub>2</sub> layer. Also, the conduction band offset (CBO) at the absorber/CdS interface is significantly reduced, which may improve the FF. However, a second “new” interface is formed between CuInSe<sub>2</sub> and CuInS<sub>2</sub>. This interface may also be defect-rich, which would be detrimental, because an even more reduced type-inversion is present here. In addition,

holes see a relatively small barrier toward this interface. Yet, if the total interface recombination (including both interfaces) would increase significantly, the gain in  $V_{OC}$  by S-incorporation would not have been observed. Thus, it is suggested that the CuInSe<sub>2</sub>/CuInS<sub>2</sub> interface is relatively benign in terms of recombination. Still, it cannot be ruled out that the significant CBO creates an electron transport barrier. This becomes more crucial with increasing CuInS<sub>2</sub> thickness (i.e., higher  $T_s$  and  $t_s$ ) because the effective barrier for thermionic emission across the CBO ( $\phi_b = E_C - E_F$ ) increases when the interface moves into a region of less band-bending. This may result in a severe reduction in FF and in a voltage-dependent photocurrent that even affects  $J_{SC}$ .

Other aspects that could explain the reduced EQE with more S-incorporation are a lowered effective bulk diffusion length  $L_n$  (i.e., by Shockley–Read–Hall recombination at grain boundaries or inside grains) or less absorption by a reduced absorber volume with pure CuInSe<sub>2</sub> composition.

A powerful tool to analyze the origin of collection losses is measuring the EQE under a negative and positive voltage bias. This was done at  $V_{bi} = -0.5$  V and  $+0.3$  V for the reference and the sample sulfurized for 15 min at 530 °C (see Figure 4a,b).

The carrier collection for the reference sample is basically unaffected by the V-bias (slight increase for  $\lambda < 520$  nm presumably artifact by photodoping in CdS<sup>[47]</sup>), which indicates that no electrical  $J_{SC}$  losses are present. In contrast, the sulfurized sample shows a slight increase under negative bias and a significant

decrease under forward bias. Figure 4c shows the corresponding EQE under V-bias normalized to the non-biased EQE. The gain under negative bias and the loss under forward bias are increasing with  $\lambda$ . This strongly indicates a severe reduction in  $L_n$  after sulfurization, which also agrees well with the trends in Figure 2b.

If a transport barrier or a pronounced recombination at the CuInSe<sub>2</sub>/CuInS<sub>2</sub> interface would limit carrier collection, a decreasing EQE with increasing  $V_{bi}$  would be expected as well, but the loss would be rather independent of  $\lambda$ .<sup>[48]</sup> A minor  $\lambda$ -dependency would still be observed because the potential transport barrier and/or harmful interface lies at some distance in the photoactive absorber material (i.e., lower collection for higher  $\lambda$ ). However, a clear kink in EQE would be expected at the band gap value of CuInS<sub>2</sub> ( $E_G = 1.53$  eV;<sup>[4]</sup> i.e., strongly reduced collection underneath CuInS<sub>2</sub>) if a transport barrier would be the main origin of the collection losses, which is obviously not the case (see Figure 2a,b).

Thus, it is suggested that a lowered  $L_n$  is the main reason for the observed trends in  $J_{SC}$  in Table 1, which also explains the greater V-dependence of the photocurrent, expressed by the lower  $R_{SH}$  for sulfurized samples. However, for a purely  $L_n$ -limited collection a larger gain at  $V_{bi} = -0.5$  V would have been expected and an additional contribution by another effect cannot be fully excluded.

To estimate the extent of the reduction in  $L_n$ , the EQEs of the Ref and S @ 530 °C samples were fitted by

$$EQE(\lambda) = (1 - R_{tot}(\lambda)) \cdot A_{par}(\lambda) \int_0^{d_{abs}} \alpha_{abs}(\lambda) \cdot \exp(-\alpha_{abs}(\lambda) \cdot x) \cdot f_C(x) dx \quad (1)$$

For the sake of convenience, the absorption coefficients for the absorber ( $\alpha_{abs}(\lambda)$ ) were taken from data for pure CuInSe<sub>2</sub>,<sup>[49]</sup> which is a fair first approximation, because the upper  $\approx 500$  nm are Ga-free. Standard absorption coefficients were used to calculate parasitic absorption in the window and buffer layer ( $A_{par}$ ) and a constant total reflection ( $R_{tot}$ ) of 8% is assumed. The expression for the collection function ( $f_C(x)$ ) is derived from ref. [50], assuming a back surface recombination velocity of  $S_{bc} = 10^4$  cm s<sup>-1</sup>, a SCR width of  $W_{SCR} = 200$  nm, and an absorber thickness of  $d_{abs} = 2.1$   $\mu$ m. The back surface field was neglected.

The resulting fits for  $L_n = 250$  and 800 nm, shown in Figure 5a, accurately reproduce the measurement data. This further indicates that a low diffusion length is the main  $J_{SC}$  limitation after sulfurization and other effects like a reduced absorption play a minor role. Figure 5b shows the corresponding collection functions and the normalized total generation rate ( $G^n$ ) for  $\lambda = 520$ –1360 nm (i.e., assuming no parasitic absorption) derived from ref. [49]. Most of the charge carriers are generated inside the SCR, where a perfect collection is assumed. If the model is accurate, collection outside the SCR is expected to be very low after sulfurization, whereas the Ref sample would exhibit significant collection in the bulk. The collection functions will be compared with electron beam-induced current (EBIC) profiles along absorber cross sections in the next section.

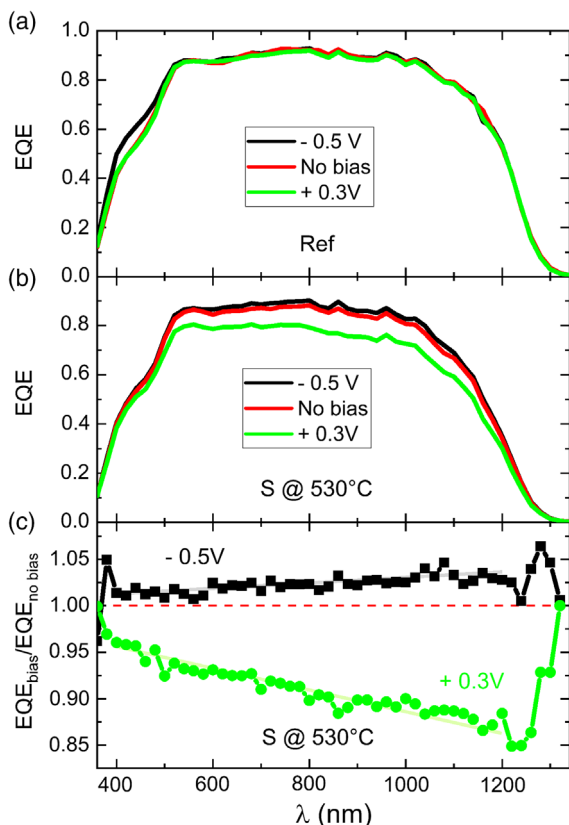


**Figure 4.** EQE under negative and positive voltage bias for the a) Ref and b) S @ 530 °C sample. c) Effect of the V-bias normalized to the non-biased measurement for S @ 530 °C.



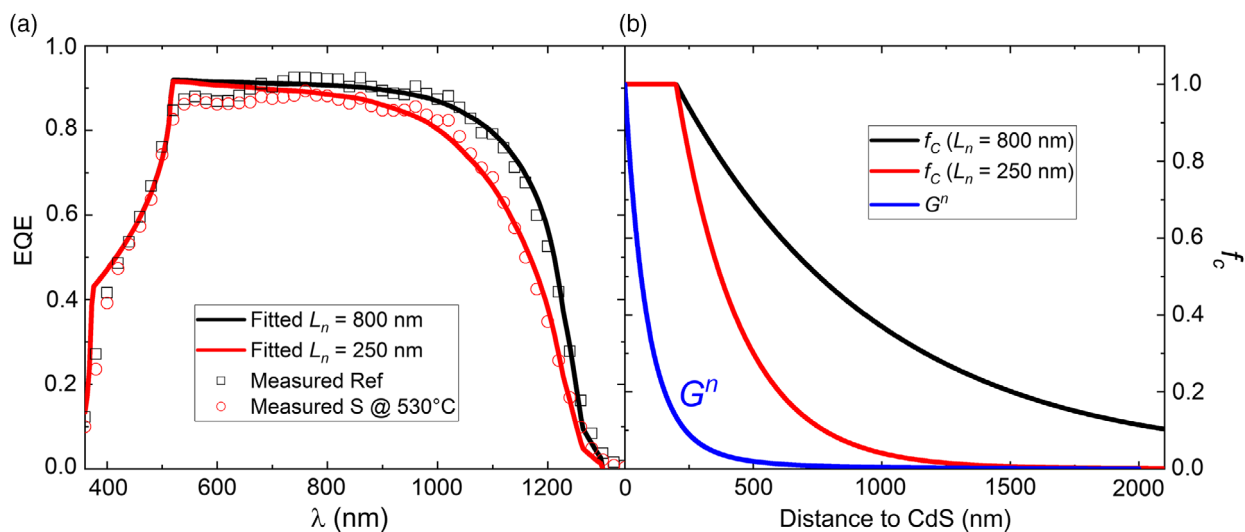


**Figure 5.** a) EQE fitted for different diffusion lengths and measured for the Ref and S @ 530 °C sample. b) Corresponding collection functions and normalized generation function deduced for  $\lambda = 520\text{--}1360$  nm from ref. [49].

## 2.2. Effect of Alk-PDT on the Performance of Solar Cells with Sulfurized Absorbers

As shown already by Feurer et al.,<sup>[8]</sup> an Alk-PDT can be beneficial for CIGS layers with a very similar elemental depth profile as used in this study (i.e., no Ga at the surface, but toward the back contact), mainly by allowing for a reduced CdS thickness and by a slight increase in  $V_{OC}$ . To verify this effect on the non-sulfurized absorbers in this study, an additional reference sample (Ref\_2) was produced (same CGI, GGI, and Ga profile as Ref) and subsequently subjected to a RbF-PDT for 173 s without chalcogenide background atmosphere to ensure direct comparability. The absence of Se (or S) during Alk-PDT has previously been shown to be non-detrimental and might even be beneficial in some cases,<sup>[43,51]</sup> which is confirmed by the results for the Ref\_2 sample in this study. As no intermediate S-step in a separate chamber was done, air exposure could be avoided until CdS deposition. The resulting cell parameters are shown in **Table 2**. Indeed, a boost in  $V_{OC}$  and FF is achieved, resulting in an efficiency of  $\eta = 18.6\%$  without antireflective coating. This is a state-of-the-art value for a low- $E_C$  chalcogenide absorber with a pure CuInSe<sub>2</sub> surface and proves that an Alk-PDT can be very beneficial for the non-sulfurized reference sample.

In the following it shall be investigated if the same boost in efficiency can be obtained after Alk-PDT on sulfurized CIGS. As distinct changes in reaction behavior for CuInSe<sub>2</sub> surfaces as compared with CuInSe<sub>2</sub> cannot be excluded, different Alk-PDT times were tested, including the standard (i.e., optimum) times used for non-sulfurized CIGS (underlined). The resulting  $I$ – $V$  characteristics for RbF- and KF-PDTs are shown in **Figure 6a,b**, respectively, and the device parameters are added to Table 2.

Obviously, no boost in efficiency was achieved by the Alk-PDTs applied on the post-sulfurized CIGS. In contrast, distinct losses in  $V_{OC}$  and FF are observed. However, the  $V_{OC}$  values are still slightly higher as compared with the non-sulfurized reference. As a trend, the FF appears to be decreasing with

**Table 2.** Device parameters of the best solar cells for Ref\_2 with and w/o RbF-PDT as well as for Ref and S @ 530 °C with and w/o different doses of RbF- and KF-PDTs (see Figure 6a,b).

Sample	FF [%]	$J_{SC,EQE}$ [mA cm <sup>-2</sup> ]	$V_{OC}$ [mV]	$\eta$ [%]
Ref_2	68.6	38.6	542	14.4
Ref_2 + RbF (173 s)	73.5	38.3	661	18.6
Ref	66.7	38.9	542	14.1
S @ 530 °C	70.9	36.5	592	15.3
S + RbF (138 s)	67.4	36.7	579	14.3
S + RbF (173 s)	66.5	37.3	556	13.8
S + RbF (207 s)	65.3	36.6	569	13.6
S + KF (20 s)	69.3	37.3	574	14.8
S + KF (225 s)	67.5	37.0	568	14.2
S + KF (300 s)	66.8	35.8	566	13.5
S + KF (375 s)	67.2	35.4	566	13.5

increasing Alk-PDT time (disregarding the S + KF (375 s) sample). The reason is a distortion in the  $I$ – $V$  curve, a so-called “kink.” Interestingly, the distortion is more severe for the Alk-PDT with the heavier alkali metal Rb. Similar behavior in  $I$ – $V$  was reported before for too strong alkali doses<sup>[28,51,52]</sup> or if a heat-treatment is done after the PDT step.<sup>[53]</sup> Different explanations were suggested for these observations. Heavy alkali species may replace Na at the interface to the Mo or MoSe<sub>2</sub> back contact, which could lead to a larger back contact barrier.<sup>[38]</sup> Others attribute the distortion to a transport/injection barrier located at the heterojunction interface(s).<sup>[28,52]</sup> Remarkably, already after a KF-PDT as short as 20 s a significant loss in  $V_{OC}$  is observed. Thus, the results prove that the post-sulfurized CIGS absorbers are much more sensitive to the Alk-PDT (for both alkali species shortest doses result in least deterioration)

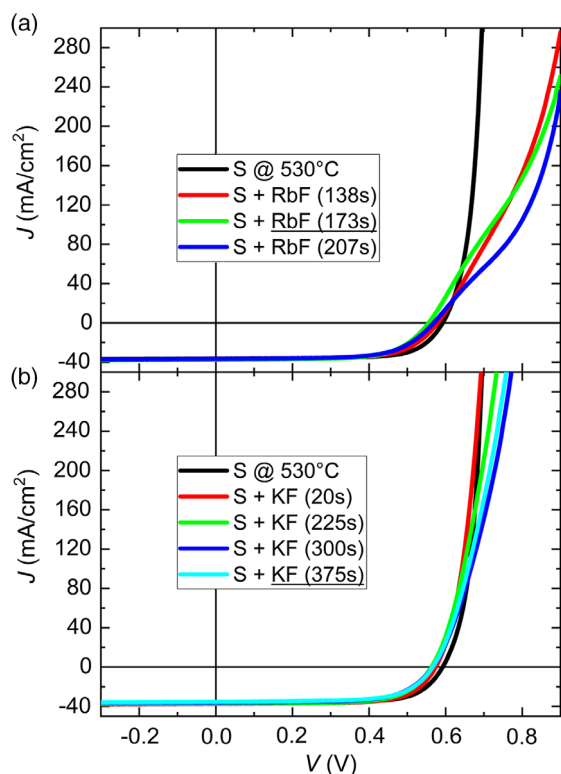


**Figure 6.**  $I$ - $V$  characteristics of the best solar cells for the S @ 530 °C sample without Alk-PDT and after different times of a) RbF- and b) KF-PDTs.

and no optimized process, leading to an efficiency improvement, was found in this study.

Apart from the mentioned negative effects, an increased  $J_{SC,EQE}$  was measured for most of the samples after Alk-PDT. **Figure 7a-d** compares the corresponding EQE spectra to the Ref and S @ 530 °C samples without Alk-PDT. For both alkali metal treatments, a significantly improved EQE for long wavelengths is measured. Here, the EQE spectra are approaching the level of the reference sample, strongly indicating an improved collection by an increased  $L_n$ . However, in the case of a KF-PDT, losses for  $\lambda < 800$  nm occur for times  $\geq 300$  s, presumably by a higher recombination rate at the heterojunction or in the CuInS<sub>2</sub> layer ( $\lambda_{Eg,CuInS_2} \approx 810$  nm).

To investigate the charge carrier collection function more directly and independent of the optical properties of the absorber, EBIC measurements were conducted on cleaved cross sections of the Ref, S @ 530 °C, and S @ 530 °C + RbF (207 s) samples. All samples were cleaved at the same time, so that differences in surface oxidation before the EBIC measurements can be excluded. Furthermore, the exact same settings were applied (e.g., magnification, working distance, etc.). The results are shown as an overlay with the scanning electron microscope (SEM) image and as an isolated EBIC map in **Figure 8a**.

Although the EBIC signal on fractured (non-polished) cross sections is strongly affected by the topography and other artifacts,<sup>[54]</sup> distinct differences between the samples are detected, indicating a significantly changed carrier collection. All samples show a similar maximum in EBIC signal close to

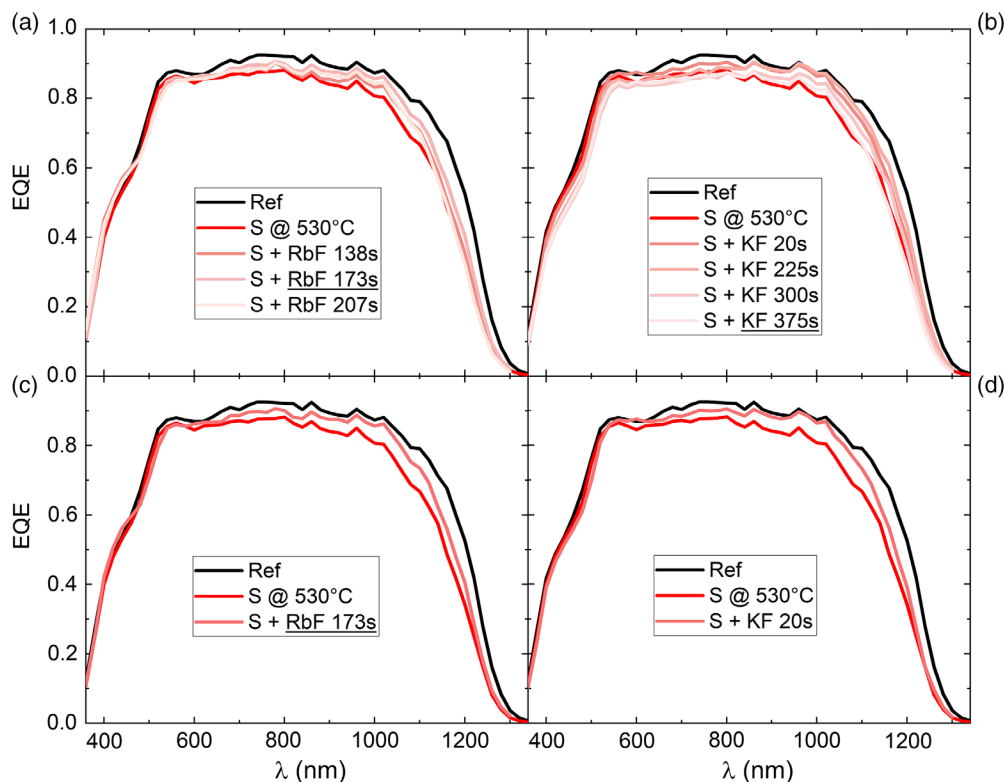


**Figure 7.** EQE spectra of the best solar cells after different times of Alk-PDT with a) RbF and b) KF compared with the Ref and S @ 530 °C samples w/o Alk-PDT. Underneath, the same spectra are illustrated, but showing only the Alk-PDT samples with the highest  $J_{SC,EQE}$  for c) RbF and d) KF, respectively.

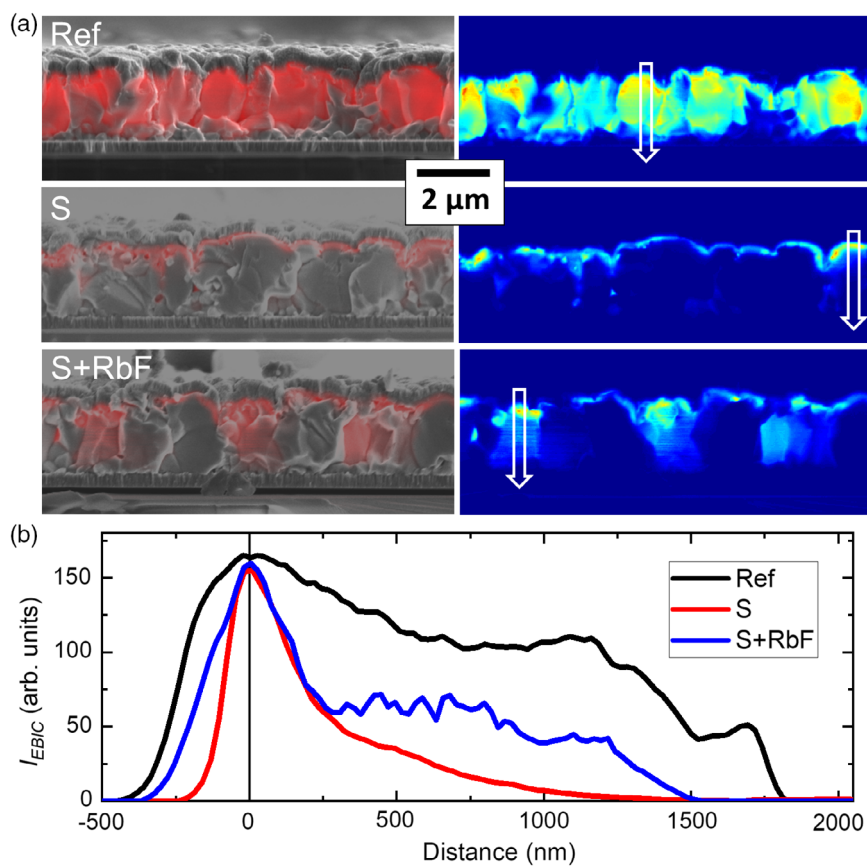


**Figure 8.** a) Electron-beam-induced current maps for the Ref, S @ 530 °C, and S @ 530 °C + RbF (207 s) samples as an overlay with SEM image and isolated. b) Corresponding line scans at the positions marked by the white arrows in part (a).

the heterojunction, most likely corresponding to perfect collection in the SCR. However, only the non-sulfurized reference sample shows a relatively homogenous and high carrier collection in the absorber bulk. This confirms again the negligible electronic  $J_{SC}$  loss for the reference, as suggested earlier. After sulfurization, the collection probability outside the SCR becomes very low. By the subsequent RbF-PDT, the collection can be significantly enhanced again in some grains, although the level of the reference is not reached. As these results were obtained very locally, EBIC was measured at several other positions and wider cross sections (see Figure S1, S2, Supporting Information). The observed features and trends are the same as shown in Figure 8a, which highlights their validity. Figure 8b shows EBIC line scans across the positions marked by the white arrows in Figure 8a, adjusted to the EBIC maximum. The electron generation profile at  $V_{acc} = 5$  kV laterally extends about 120 nm in CIGS.<sup>[55]</sup> Thus, as a first approximation the EBIC profile should roughly match the collection function  $f_C(x)$ . Indeed, the EBIC line scans for the Ref and sulfurized samples w/o RbF-PDT are comparable with the  $f_C(x)$  as calculated for the different diffusion lengths in Figure 5b. This again strengthens the assumption that the  $J_{SC}$  losses after sulfurization are not explainable by a transport barrier or an increased interface recombination, but originate from a reduced  $L_n$ . However, it cannot be fully excluded that a reduction in  $W_{SCR}$  by a potentially higher doping in the

CuInS<sub>2</sub> contributes as well. Indeed, for stoichiometric CuInS<sub>2</sub> a very high hole density of  $\approx 1 \times 10^{17} \text{ cm}^{-3}$  was reported (while Cu-poor grown CuInS<sub>2</sub> suffers from very low doping).<sup>[56,57]</sup>

In the final paragraph, it is investigated how the heavy alkali metals are incorporated into sulfurized CIGS, to understand the observed changes after Alk-PDT (e.g., the “selective grain activation” with respect to carrier collection or the current blocking).

### 2.3. Analysis of Heavy Alkali Metal Incorporation into Sulfurized CIGS Absorbers

Figure 9 shows the depth distribution of Rb (Figure 9a) and K (Figure 9b) after different times of Alk-PDT on the S @ 530 °C sample as measured by GDOES. The Ref sample is added in (Figure 9a) to estimate the noise level. In both cases, the Cd and Mo signals are shown for one of the samples subjected to Alk-PDT. As expected, longer Alk-PDT times result in an increased incorporation of alkalis. All samples show an agglomeration at the Mo back contact and toward the heterojunction. After a RbF-PDT time  $\geq 173$  s, a Rb-peak at or close to the absorber/buffer interface evolves. After the concentration declined toward the bulk, it reaches a rather constant level, which is similar for all times of RbF-PDT and distinctly higher as the measurement noise (compare signal for Ref). It was found that Rb exclusively diffuses through random, high-angle GBs if Na is

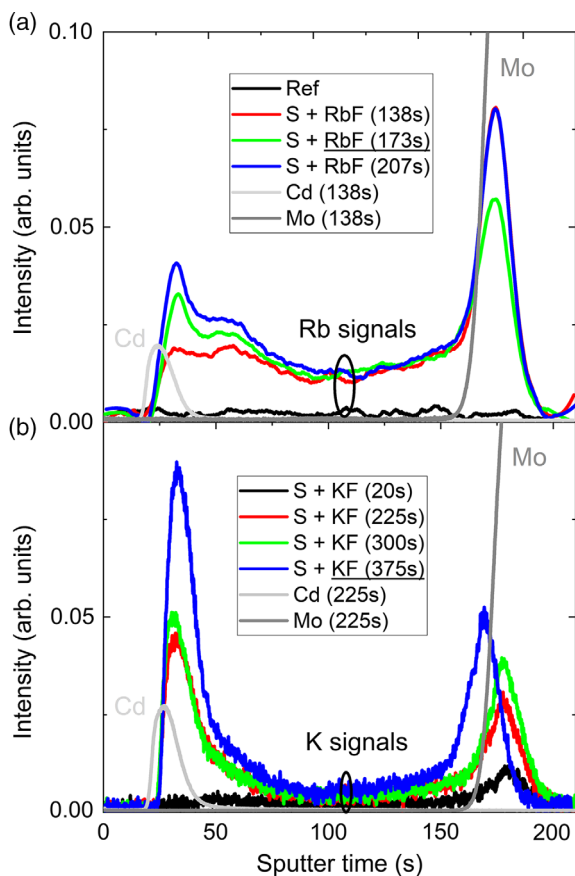


**Figure 9.** a) Rb and b) K depth profiles for different times of Alk-PDT on the S @ 530 °C sample (Ref is added in part (a) to estimate noise level) as measured by GDOES. The Cd and Mo signals for one sample of each alkali species are added as well.

present in the initial absorber (as it is the case here).<sup>[58,59]</sup> It is suggested that it pushes the lighter Na out of the GBs, although it does not easily remove Na that occupies vacancies in the lattice, which are required for migration. As a result, diffusion into the grain interior is hindered.<sup>[58]</sup>

In the case of the KF-PDT, similar trends are observed; with the difference that a higher K signal is measured in the heterojunction region as compared with the back contact interface (the very short PDT time is an exception). The reason may be that the heavier Rb pushes Na out of the GBs more easily than the lighter K, as proposed earlier,<sup>[29]</sup> thereby facilitating diffusion to the back contact. Alternatively, Rb may also replace Na at the back contact interface more easily than K.

Hence, the GDOES results can be understood as alkali metals diffusing from an unlimited source at the surface via high-angle GBs into the absorber. After some time, they reach the back contact interface, where the concentration gradually increases. However, it is unclear where the alkali peak close to the CdS layer stems from. Possible explanations are that 1) Rb/K agglomerates at the CdS/CuInS<sub>2</sub> (e.g., in the form of an Alk-In-S surface layer) or CuInS<sub>2</sub>/CuInS<sub>2</sub> interface, 2) Rb follows a regular diffusion profile which is distorted in the GDOES profile by the roughness of the interfaces, or 3) the density of GBs is higher toward the surface.

To investigate the alkali incorporation on a nanoscale, several regions, corresponding to different depths of the S @ 530 °C + RbF (207 s) sample, were analyzed by STEM-EDS mapping. The strongest RbF dose was chosen intentionally because possible modifications would be expected to be most pronounced here. **Figure 10** shows the results for the entire cross section (long shot). The features of the post-sulfurization are visible as a strong S signal, stemming from the CuInS<sub>2</sub>, and lower concentrations in regions of CuIn(S,Se)<sub>2</sub> (S signal at the back contact is an artifact by overlap with Mo line). In addition, a slight increase in Cu is observed, where S is incorporated. The graph shows the concentrations of the absorber elements averaged for each row of the EDS mappings (i.e., perpendicular to the substrate), as a kind of average depth profile.

By far the highest Rb concentration is detected at the MoSe<sub>2</sub>/absorber interface, which is in line with the GDOES results. Previous studies reported the same feature after RbF-PDT on CIGS absorbers.<sup>[59,60]</sup>

To resolve lower alkali concentrations at the heterojunction or in GBs, analysis at higher magnification is required. This was done at two positions focusing on the heterojunction (see Figure S3, S4, Supporting Information). However, no Rb was found at the CdS/CuInS<sub>2</sub> or at the CuInS<sub>2</sub>/CuInS<sub>2</sub> interface. Furthermore, no Cu-poor regions, which may indicate the presence of a (Cu,Rb)-In-S layer or clusters, could be detected at the absorber surface. Schöppe et al. recently reported that widely dispersed Cs-, In-, and Se-enriched and Cu- and Ga-depleted (possibly CsInSe<sub>2</sub>) particles formed at the absorber surface after CsF-PDT on CIGS absorbers if the sample was air exposed before PDT (as it was the case in this study). In contrast, a more homogenous distribution of Cs at the buffer interface was detected if the sample was not exposed to oxygen before PDT.<sup>[35]</sup> Even in the case of RbF-PDT on CIGS, some studies report on RbInSe<sub>2</sub> particle<sup>[61]</sup> or island<sup>[34]</sup> formation at the buffer interface, whereas others suggest a closed Rb(Na)-In-Se layer.<sup>[28]</sup> Thus, it cannot be excluded that widely dispersed Rb-containing compounds formed at the CuInS<sub>2</sub> surface, but were not captured by the ≈10 μm wide TEM lamella.

To investigate possible changes in surface composition in more detail, hard X-ray photoelectron spectroscopy (HAXPES) was conducted on the sulfurized absorber with and without RbF-PDT at photon energies of 3 and 9 keV (see Figure S5, Supporting Information). The as-prepared samples were sealed in a plastic bag under N<sub>2</sub> and transported to the synchrotron for characterization. Prior to the measurements, the samples were rinsed in water to remove salts from the surface. No significant modification in surface chemistry was found, pointing to the non-existence of a newly formed phase like Rb-In-S. Furthermore, no Rb was detected within the probing depth of ≈30 nm at 9 keV (i.e., lower than CuInS<sub>2</sub> extension), which is in line with the STEM-EDS observations and indicates that the Rb-peak close to the CdS in GDOES probably marks the beginning Rb decoration of GBs underneath the CuInS<sub>2</sub> layer.

The potential absence of a wide-gap surface phase formation after Alk-PDT might, at least partly, explain the missing *V*<sub>OC</sub> and FF improvement for the sulfurized samples.

**Figure 11** shows the STEM-EDS analysis of several GBs (and triple points) close to the absorber surface, where S is



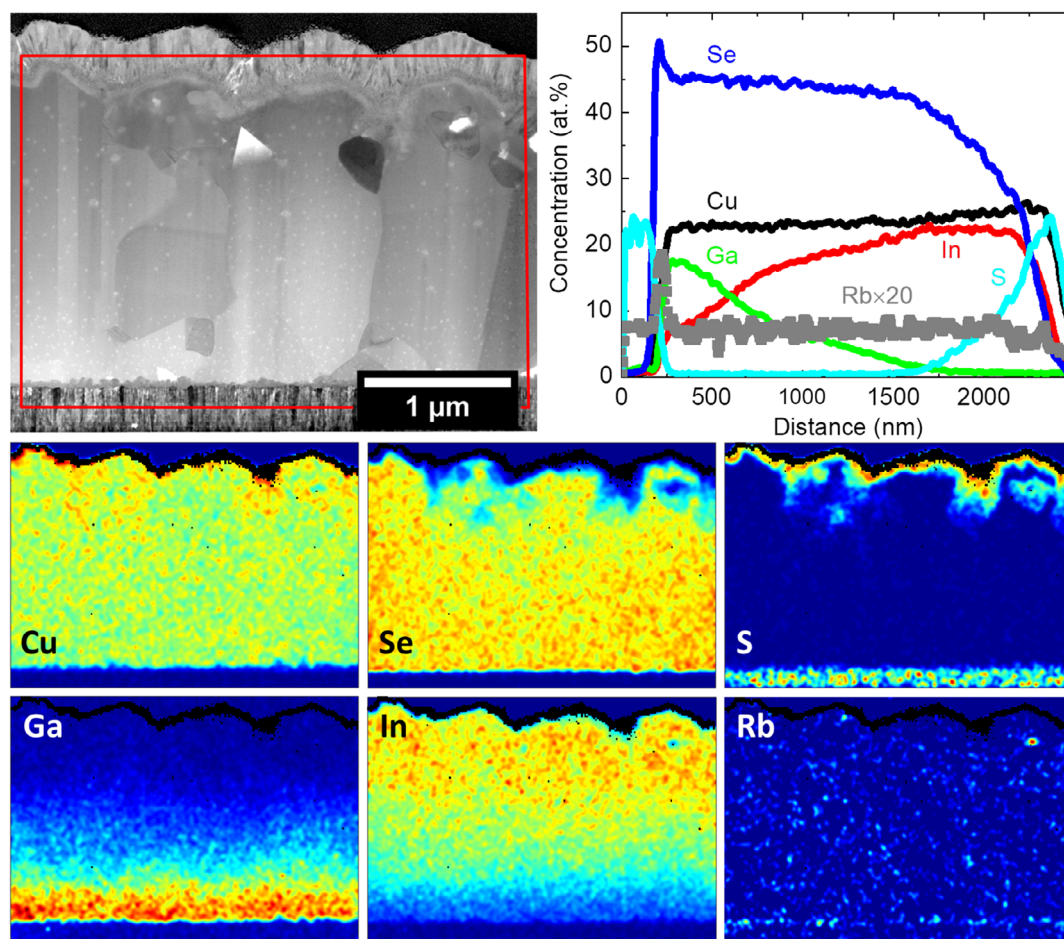


**Figure 10.** STEM BF image of the S @ 530 °C + RbF (207 s) sample. The red rectangle marks the region of the elemental EDS mapping, which results are shown underneath for the absorber elements and Rb (Cd concentration >1 at% from CdS layer is illustrated by black pixels in each map). The graph in the upper right shows the row-wise averaged atomic concentrations as extracted from the elemental maps.

incorporated and abrupt changes in S concentration from one grain to another are visible. A significant Rb agglomeration in the GBs is obvious, accompanied by a clear Cu-enrichment and In-depletion, as reported earlier for sulfurized CIGS<sup>[20,22]</sup> without Alk-PDT. The surface-near GBs are most likely Cu-enriched during sulfurization, when Cu needs to be supplied to the reaction front to incorporate S and GBs act as diffusion channels.

In the case of non-sulfurized CIGS, the agglomeration of heavy alkalis at GBs after Alk-PDT is basically always accompanied by a reduction in Cu and an increase in In content.<sup>[60,62–66]</sup> It was suggested that this could be due to the formation of an Alk–In–Se compound in the GBs that reduces GB recombination, which is supposedly the main driver for the beneficial effect of the treatment.<sup>[30,37]</sup> It may be speculated that this Alk–In–Se formation in GBs was only partially achieved on the sulfurized absorbers in this study because some GBs might be too enriched in Cu by the preceding S-step. This would explain why some grains could be “activated” (increased collection) by the Alk-PDT and others (presumably with Cu-rich GBs) could not.

It was suggested earlier that even without heavy alkali decoration Cu-depletion at GBs indicates the presence of a hole barrier that reduces recombination.<sup>[67–70]</sup> Thus, the Cu-enrichment

caused by sulfurization may in general lead to more detrimental GBs, which would also explain the significantly reduced effective diffusion length (compare Figure 8). However, it remains to be proven if Cu-enrichment of GBs always takes place during S-incorporation. Especially for sequentially processed absorbers this may not generally be the case. Although a clear correlation of S- and Cu-enrichment was found in the absorber GBs of devices with moderate performance ( $\eta \approx 15\%$ ),<sup>[22]</sup> it is not confirmed that the same feature is observed for solar cells with record efficiencies >23%.<sup>[41]</sup> In general, the S-incorporation should be less dependent on the Cu supply (i.e., no/less long-range diffusion via GBs) for sequential processes because S is incorporated during crystallization and exclusively forms mixed crystals which allows for more tolerance to off-stoichiometry than forming CuInS<sub>2</sub>.<sup>[21]</sup> Another aspect that needs further investigation is the role of sulfur in GBs where it is found to agglomerate after sulfurization. It cannot be excluded that this leads to a downward shift of the valence band maximum, which may (partially) cancel out the detrimental effect of the accompanied Cu-enrichment.

To investigate if the Cu-enrichment is also present in GBs far away from the surface (where Cu-stoichiometry was needed for

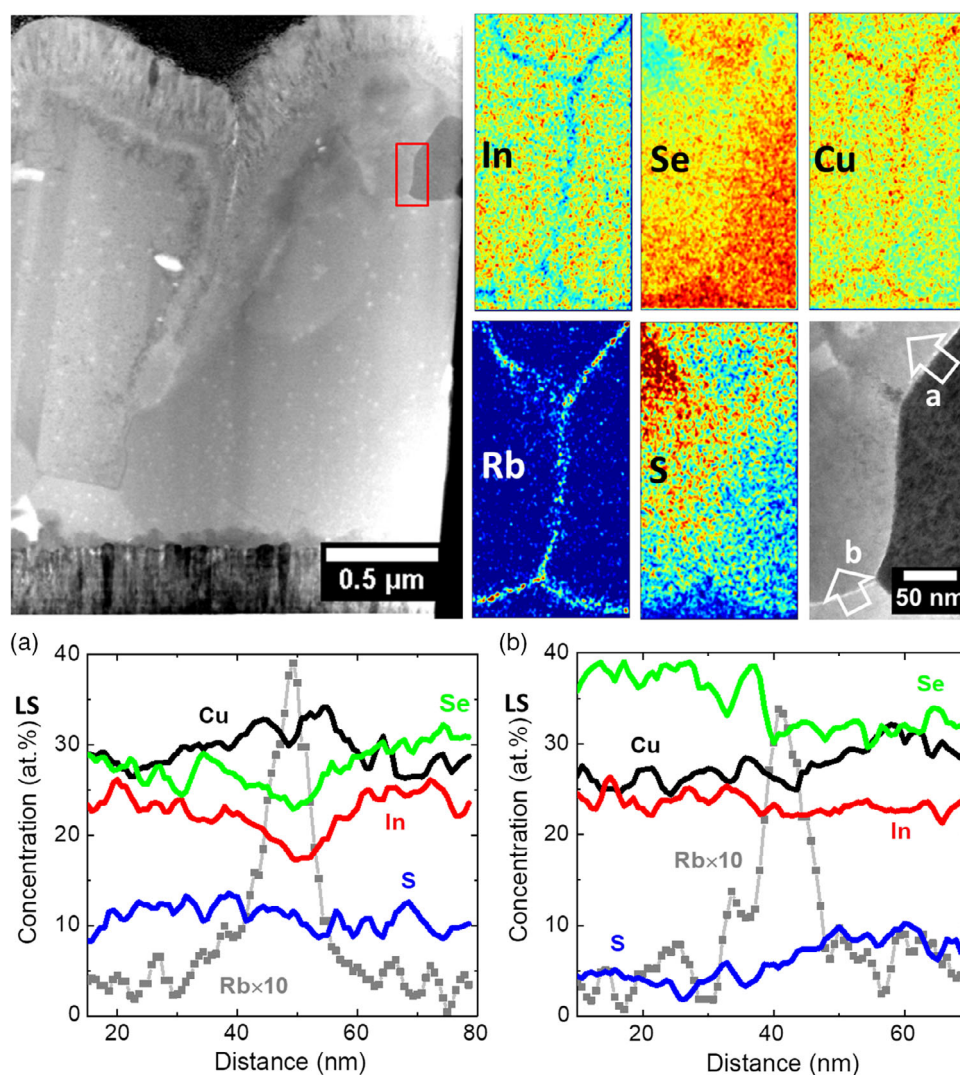


**Figure 11.** STEM BF image of the S @ 530 °C + RbF (207 s) sample. The red rectangle marks the region of the elemental EDS mapping, which results are shown on the right-hand side for the absorber elements and Rb. The graphs underneath show line scans extracted from the EDS mappings across GBs, as indicated by the white arrows “a” and “b” in the BF image above.

S-incorporation), STEM-EDS analysis was done at the interface to the back contact (see **Figure 12**). Clearly, the analyzed GBs are not enriched, but rather depleted in Cu. Again, Rb is found in the GBs. However, it is impossible to judge if the Alk-PDT led to the Cu-depletion (e.g., by forming an Alk–In–Se compound) or if GBs close to the back contact were generally not Cu-enriched during sulfurization because Cu could be supplied from absorber material closer to the surface. Nevertheless, the findings are in line with the proposed hypothesis: an increased recombination at GBs is responsible for the observed losses in carrier collection and reduced  $J_{SC}$  after sulfurization. After Alk-PDT some of the Cu-enriched GBs can be, at least partly, turned into Cu-depleted GBs and are thereby passivated. As a consequence, some grains exhibit an increased carrier collection, as observed in the EBIC measurements, and  $J_{SC}$  can be slightly increased again. Further analysis and more statistics are necessary to confirm this hypothesis.

Still, it is not clear why the Alk-PDT on sulfurized CIGS led to  $V_{OC}$  and FF losses. As shown in **Figure 12**, Rb strongly agglomerates at the CIGS/MoSe<sub>2</sub> interface. Pianezzi et al. suggested that a replacement of Na by heavier alkalis at the back contact interface increases the barrier height.<sup>[38]</sup> Indeed, a significantly reduced Na signal at the back (and also at the front) contact interface is observed after Alk-PDT as measured by GDOES (Na peaks vanish; see **Figure S6**, Supporting Information). Therefore, it is proposed that a back contact barrier is the reason for the distortion in  $I$ – $V$  and the FF losses after Alk-PDT on sulfurized absorbers. This would also explain why less blocking is observed after KF-PDT as compared with RbF-PDT because a lower concentration of K than Rb is suspected at the CIGS/MoSe<sub>2</sub> interface (compare **Figure 9**). Indeed, a lower Na content is measured close to and in the Mo layer itself after the RbF-PDT as compared with the KF-PDT (see **Figure S6**, Supporting Information). Nevertheless, this finding needs to be confirmed by more



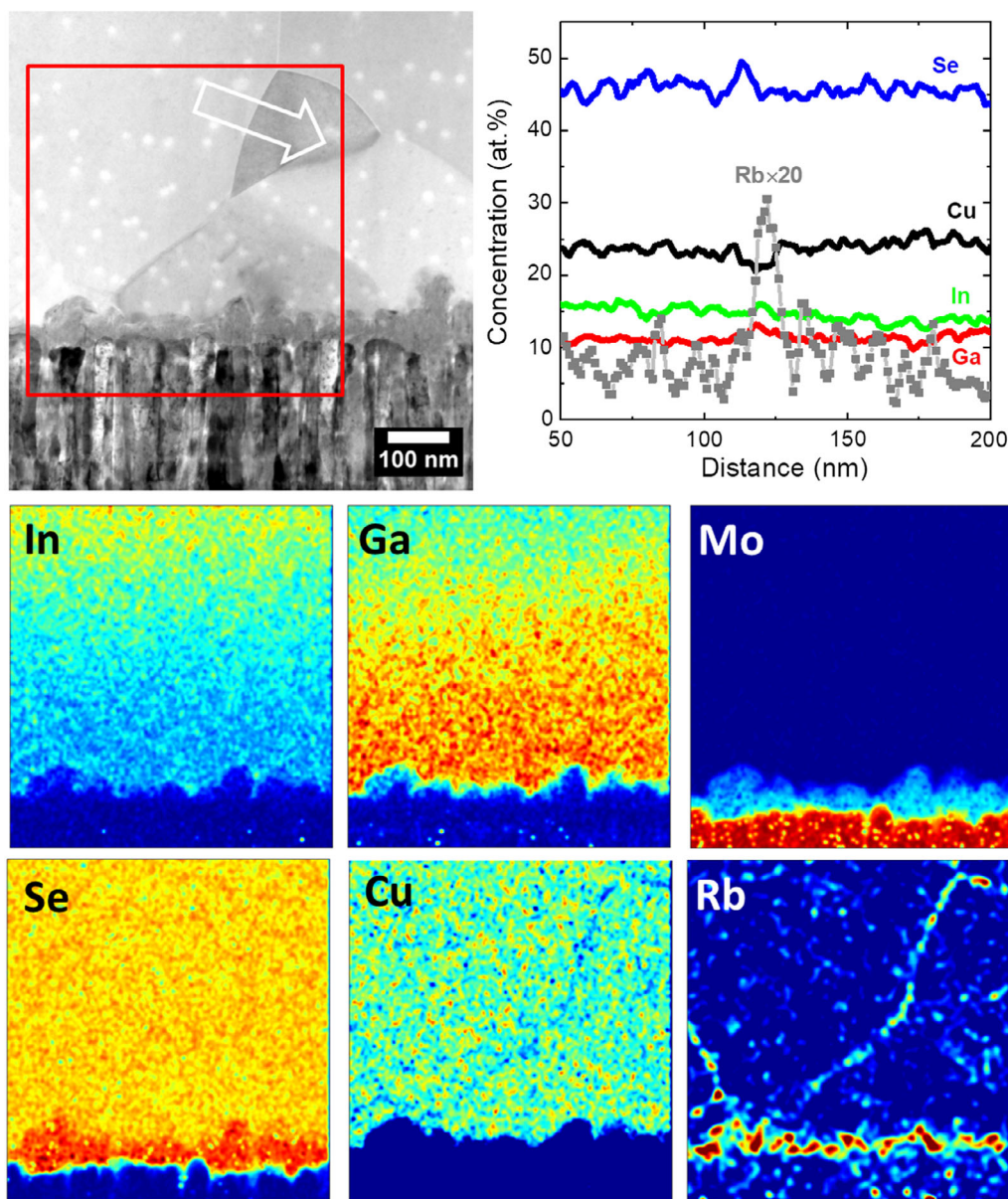


**Figure 12.** STEM BF image of the back contact region of the S @ 530 °C + RbF (207 s) sample. The red rectangle marks the region of the elemental EDS mapping, which results are shown underneath for the absorber elements as well as Rb and Mo. The graph shows the line scan extracted from the EDS mappings across the GB, as indicated by the white arrow in the BF image.

quantitative methods like secondary ion mass spectroscopy in the future. However, at this point it is not clear why this barrier established for the sulfurized CIGS, while no blocking was observed on the non-sulfurized sample subjected to Alk-PDT.

The question remains why no  $V_{OC}$  improvement was obtained. Considering the improved collection efficiency after Alk-PDT, a gain in  $V_{OC}$  would be expected but instead, even a  $V_{OC}$  loss is observed. A possible explanation could be that apparently no surface modification was induced by the Alk-PDT. This may be due to the lack of Ga at the surface to form  $GaF_3$  and thereby reducing the surface<sup>[71]</sup> (although this would account for the non-sulfurized sample as well) or because an Alk-In-S

compound is less likely to form than Alk-In-Se. Indeed, a significant S reduction was observed at the surface after KF-PDT of a  $Cu(In,Ga)(S,Se)_2$  absorber,<sup>[42]</sup> which would agree with the latter point. The intolerance to off-stoichiometry for  $CuInS_2$  (i.e., does not allow to be reduced in Cu) may further explain a reaction inertness when exposed to alkali fluorides. However, in a previous study on post-sulfurized CIGS (in  $H_2S$ ), which also resulted in a pure  $CuInS_2$  surface, a  $V_{OC}$  and efficiency gain is reported after KF-PDT.<sup>[43]</sup>

It cannot be excluded that the air exposure between sulfurization and subsequent Alk-PDT ( $\approx 30$  min) may be the origin of the performance deterioration. In an attempt to prevent oxidation,

the absorber was capped by CdS, which was selectively removed by etching in HCl right before Alk-PDT. However, it turned out that HCl etching damaged the newly formed CuInS<sub>2</sub> layer (while no detrimental etching effect was observed for non-sulfurized CIGS). In future experiments, the air exposure time will be either minimized or completely avoided by performing the sulfurization and Alk-PDT in the same vacuum chamber.

Finally, this study illustrates the potential of combining a post-sulfurization of co-evaporated CIGS with an Alk-PDT step. However, it also highlights the challenges to achieve a similar  $V_{OC}$  and FF boost by the Alk-PDT for sulfurized CIGS as it is seen for a non-sulfurized absorber. If remaining obstacles can be overcome in the future, the “Alk-PDT after sulfurization” post-processing is a promising route to produce high efficiency low- $E_C$  solar cells for application in tandem devices.

### 3. Conclusion

This work studies the applicability of a heavy alkali fluoride treatment on post-sulfurized CIGS absorbers processed by co-evaporation. It is shown that sulfurization can improve the efficiency of low-gap CIGS solar cells by increasing  $V_{OC}$  and FF. However, a loss in  $J_{SC}$  is observed upon incorporation of S, which limits its benefit. It is proposed that this effect is caused by a reduced effective diffusion length, due to an increased grain boundary recombination. This, in turn, is ascribed to Cu-enrichment of GBs during sulfurization, when Cu is transported via GBs to the surface to allow S-incorporation.

After RbF- or KF-PDT, carrier collection can be increased for some grains, which potentially mitigates the  $J_{SC}$  loss after sulfurization. An explanation for the “selective activation” of grains after Alk-PDT may be that some GBs can be passivated by the alkali decoration (e.g., by forming an Alk-In-Se(S) compound), while other, potentially too Cu-enriched GBs remain Cu-rich and thereby detrimental. However, in strong contrast to non-sulfurized CIGS, for which a state-of-the-art efficiency of 18.6% could be achieved, the Alk-PDT did not result in an efficiency improvement for sulfurized CIGS. Here, a distortion in  $I$ - $V$  characteristics is accompanied by losses in  $V_{OC}$  and FF. No surface modification was observed after RbF-PDT, which may be attributed to air exposure between the sulfurization and Alk-PDT processing steps. Alternatively, the CuInS<sub>2</sub> surface may be more inert than CuInSe<sub>2</sub> during Alk-PDT (e.g., AlkInSe<sub>2</sub> favored over AlkInS<sub>2</sub> formation). The absence of a wide-gap phase at the surface may explain why the Alk-PDT did not result in an increased  $V_{OC}$  for sulfurized CIGS. It is further suggested that a back contact barrier is formed when replacing Na by heavier alkalis at the CIGS/MoSe<sub>2</sub> interface, which is responsible for the distortion in  $I$ - $V$  and may at least partially account for the FF loss.

### 4. Experimental Section

**Solar Cell Processing:** The CIGS solar cells were processed in the following stack sequence: soda lime glass (SLG)/Mo/NaF/CIGS(+post-sulfurization)(+Alk-PDT)/CdS/i-ZnO/ZnO:Al. First, the Mo back contact was deposited on the cleaned SLG substrate ((12.5 × 12.5) cm<sup>2</sup>) by DC-sputtering (i.e., no Na-diffusion barrier between SLG and Mo). Subsequently, a 10 nm-thick NaF layer was grown on top by thermal

evaporation. In the next step, the CIGS absorber was deposited using a three-stage co-evaporation process (Cu-poor → Cu-rich → Cu-poor). Gallium was only evaporated during the first and In mainly during the third stage to create a strong elemental grading and a corresponding band gap increase toward the back contact. The rates were adjusted in a way that the final absorber is Ga-free at the surface, corresponding to a very similar Ga depth profile as in our previous sulfurization study.<sup>[17]</sup> The average, integral  $[Ga]/([Ga]+[In]) = CGI$  and  $[Cu]/([Ga]+[In]) = CGI$  values for the samples are  $CGI = 0.23 \pm 0.01$  and  $0.89 \pm 0.02$ , respectively. The final absorber thickness is 2.1 μm (± 0.1 μm).

After absorber formation, the samples were coated with a 50 nm CdS layer by chemical bath deposition (CBD) to prevent degradation before subsequent post-sulfurization runs. Just before each sulfurization experiment, all samples were etched in 4 M HCl for 60 s to remove the CdS cap (air exposure <2 min). The samples were subjected to annealing in elemental S-atmosphere at an Ar pressure of 50 mbar in a customized vacuum furnace. In total, five different sulfurization conditions were tested, with annealing temperatures ( $T_s$ ) ranging from 460 to 560 °C and times ( $t_s$ ) from 15 to 40 min. Further details about the sulfurization system can be found in ref. [16]. To study the effect of the Alk-PDT on the sulfurized CIGS absorber, several samples subjected to the same 15 min S-anneal at 530 °C were transported to a separate vacuum chamber (air exposure ≈ 30 min). Here, RbF- and KF-PDTs were performed for different times (including standard times for non-sulfurized CIGS) at substrate temperatures of 333 and 339 °C, respectively. The deposition rates were adjusted by the source temperature and controlled by quartz crystal microbalance monitoring. No chalcogenide (i.e., S or Se) was co-evaporated during the Alk-PDT.

All samples were finalized by adding a 50 nm CdS (CBD) buffer layer and a sputtered bilayer of i-ZnO(70 nm)/ZnO:Al(210 nm). For the sake of comparability, it was avoided to use a thinner buffer layer for the alkali-treated samples. In the end, 25 solar cells with an area of  $A = 0.05$  cm<sup>2</sup> were sectioned by mechanical scribing. Equivalent reference devices without a sulfurization step (“Ref”), but with CdS removal and redeposition, were processed accordingly.

**Microstructural and Chemical Absorber Characterization:** GDOES, using a Spectra Analytik GDA 750HR system, was conducted to investigate the alkali distribution in the absorber films. STEM on a FEI Titan Themis XFEI instrument assisted by EDS allowed for nanoscale investigation of Rb segregation after RbF-PDT and identification of chemical modifications after S-incorporation. HAXPES measurements were performed at the GALAXIES undulator beamline of the Soleil synchrotron (France). The spectra were recorded using excitation energies of 3 and 9 keV and using a VG Scienta EW4000 energy electron analyzer at normal emission. A pass energy of 200 eV was used for all measurements, and the binding energy was calibrated by measuring the 4f spectrum of a grounded Au foil and setting the Au 4f<sub>7/2</sub> binding energy to 84.0 eV.

**Characterization of Solar Cells:** Completed solar cell devices were characterized by EQE measurements and by  $I$ - $V$  analysis at  $T = 25$  °C under illumination by an ELH lamp in home-built setups. The light intensity for the  $I$ - $V$  measurements was calibrated to the  $J_{SC,EQE}$  at AM1.5G conditions as deduced from EQE. EBIC measurements were conducted on cleaved solar cell cross sections in a FEI Helios Nanolab SEM at an acceleration voltage of  $V_{acc} = 5$  kV and a beam current of 86 pA.

### Supporting Information

Supporting Information is available from the Wiley Online Library or from the author.

### Acknowledgements

This work was supported by the Swedish foundation for strategic research (SSF) under the project number RMA15-0030 and the StandUp for Energy program. The authors acknowledge SOLEIL for time on GALAXIES



beamline under proposal ID 20181721. Support from Dr. Jean-Pascal Rueff at the Beamline is also acknowledged.

## Conflict of Interest

The authors declare no conflict of interest.

## Keywords

Cu(In,Ga)Se<sub>2</sub>, grain boundaries, KF-post-deposition treatments, RbF-post-deposition treatments, sulfurization

Received: May 15, 2020

Revised: June 3, 2020

Published online:

- [1] V. Probst, W. Stetter, W. Riedl, H. Vogt, M. Wendl, H. Calwer, S. Zweigart, K.-D. Ufert, B. Freienstein, H. Cerva, F. H. Karg, *Thin Solid Films* **2001**, 387, 262.
- [2] T. Kato, J. Wu, Y. Hirai, H. Sugimoto, V. Bermudez, *IEEE J. Photovolt.* **2019**, 9, 325.
- [3] T. Kobayashi, H. Yamaguchi, Z. Jehl, L. Kao, H. Sugimoto, T. Kato, H. Hakuma, T. Nakada, *Prog. Photovolt. Res. Appl.* **2015**, 23, 1367.
- [4] S.-H. Wei, A. Zunger, *J. Appl. Phys.* **1995**, 78, 3846.
- [5] U. Rau, M. Schmitt, F. Engelhardt, O. Seifert, J. Parisi, W. Riedl, J. Rimmasch, F. Karg, *Solid State Commun.* **1998**, 107, 59.
- [6] M. Beres, K. M. Yu, J. Syzdek, S. S. Mao, *Thin Solid Films* **2016**, 608, 50.
- [7] Q. Han, Y.-T. Hsieh, L. Meng, J.-L. Wu, P. Sun, E.-P. Yao, S.-Y. Chang, S.-H. Bae, T. Kato, V. Bermudez, Y. Yang, *Science* **2018**, 361, 904.
- [8] T. Feurer, F. Fu, T. P. Weiss, E. Avancini, J. Löckinger, S. Buecheler, A. N. Tiwari, *Thin Solid Films* **2019**, 670, 34.
- [9] M. Jost, T. Bertram, D. Koushik, J. A. Marquez, M. A. Verheijen, M. D. Heinemann, E. Kohnen, A. Al-Ashouri, B. Rech, T. Unold, M. Creatore, I. Laueremann, C. A. Kaufmann, R. Schlatmann, S. Albrecht, in *IEEE 46th Photovoltaic Specialists Conf.*, IEEE, Chicago, IL **2019**, pp. 738–742.
- [10] A. S. Brown, M. A. Green, *Physica E* **2002**, 14, 96.
- [11] <https://www.nrel.gov/pv/cell-efficiency.html> (accessed: 10 May 2020).
- [12] T. Nakada, H. Ohbo, T. Watanabe, H. Nakazawa, M. Matsui, A. Kunioka, *Sol. Energy Mater. Sol. Cells* **1997**, 49, 285.
- [13] J. Keränen, J. Lu, J. Barnard, J. Sterner, J. Kessler, L. Stolt, Th. W. Matthes, E. Olsson, *Thin Solid Films* **2001**, 387, 80.
- [14] U. P. Singh, W. N. Shafarman, R. W. Birkmire, *Sol. Energy Mater. Sol. Cells* **2006**, 90, 623.
- [15] D. Ohashi, T. Nakada, A. Kunioka, *Sol. Energy Mater. Sol. Cells* **2001**, 67, 261.
- [16] J. K. Larsen, J. Keller, O. Lundberg, T. Jarmar, L. Riekehr, J. J. S. Scragg, C. Platzer-Bjorkman, *IEEE J. Photovolt.* **2018**, 8, 604.
- [17] J. Keller, O. V. Bilousov, E. Wallin, O. Lundberg, J. Neerken, S. Heise, L. Riekehr, M. Edoff, C. Platzer-Bjorkman, *Phys. Status Solidi A* **2019**, 2016, 1900472.
- [18] G. Wang, G. Cheng, B. Hu, X. Wang, S. Wan, S. Wu, Z. Du, *J. Mater. Res.* **2010**, 25, 2426.
- [19] B. J. Mueller, M. Mock, V. Haug, F. Hergert, T. Koehler, S. Zweigart, U. Herr, *Thin Solid Films* **2015**, 582, 284.
- [20] H. Aboulfadl, J. Keller, J. Larsen, L. Riekehr, M. Edoff, C. Platzer-Bjorkman, *Microsc. Microanal.* **2019**, 25, 532.
- [21] C. Stephan, Dissertation, Freie Universität Berlin **2011**.
- [22] J. Keller, R. Schlesiger, I. Riedel, J. Parisi, G. Schmitz, A. Avellan, T. Dalibor, *Sol. Energy Mater. Sol. Cells* **2013**, 117, 592.
- [23] A. Chirila, P. Reinhard, F. Pianezzi, P. Blösch, A. R. Uhl, C. Fella, L. Kranz, D. Keller, C. Gretener, H. Hagendorfer, D. Jaeger, R. Erni, S. Nishiwaki, S. Buecheler, A. N. Tiwari, *Nat. Mater.* **2013**, 12, 1107.
- [24] P. Reinhard, F. Pianezzi, B. Bissig, A. Chiril, P. Blösch, S. Nishiwaki, *IEEE J. Photovolt.* **2015**, 5, 656.
- [25] T. M. Friedlmeier, P. Jackson, A. Bauer, D. Hariskos, O. Kiowski, R. Wuerz, M. Powalla, *IEEE J. Photovolt.* **2015**, 5, 1487.
- [26] T. M. Friedlmeier, P. Jackson, D. Kreikemeyer-Lorenzo, D. Hauschild, O. Kiowski, D. Hariskos, L. Weinhardt, C. Heske, M. Powalla, in *IEEE 43rd Photovoltaic Specialists Conf.*, IEEE, Portland, OR **2016**, pp. 457–461.
- [27] P. Jackson, D. Hariskos, R. Wuerz, O. Kiowski, A. Bauer, T. M. Friedlmeier, M. Powalla, *Phys. Status Solidi – Rapid Res. Lett.* **2014**, 1, 28.
- [28] T. Kodalle, M. D. Heinemann, D. Greiner, H. A. Yetkin, M. Klupsch, C. Li, P. A. van Aken, I. Laueremann, R. Schlatmann, C. A. Kaufmann, *Sol. RRL* **2018**, 2, 1800156.
- [29] P. Jackson, R. Wuerz, D. Hariskos, E. Lotter, W. Witte, M. Powalla, *Phys. Status Solidi – Rapid Res. Lett.* **2016**, 586, 583.
- [30] S. Siebentritt, E. Avancini, M. Bär, J. Bombsch, E. Bourgeois, S. Buecheler, R. Carron, C. Castro, S. Duguay, R. Félix, E. Handick, D. Hariskos, V. Havu, P. Jackson, H. P. Komsa, T. Kunze, M. Malitckaya, R. Menozzi, M. Nesladek, N. Nicoara, M. Puska, M. Raghuvanshi, P. Pareige, S. Sadewasser, G. Sozzi, A. N. Tiwari, S. Ueda, A. Vilalta-Clemente, T. P. Weiss, F. Werner, et al., *Adv. Energy Mater.* **2020**, 10, 1903752.
- [31] C. P. Muzzillo, *Sol. Energy Mater. Sol. Cells* **2017**, 172, 18.
- [32] E. Handick, P. Reinhard, J. H. Alsmeier, L. Köhler, F. Pianezzi, S. Krause, M. Gorgoi, E. Ikenaga, N. Koch, R. G. Wilks, S. Buecheler, A. N. Tiwari, M. Bär, *ACS Appl. Mater. Interfaces* **2015**, 7, 27414.
- [33] E. Handick, P. Reinhard, R. G. Wilks, F. Pianezzi, T. Kunze, D. Kreikemeyer-Lorenzo, L. Weinhardt, M. Blum, W. Yang, M. Gorgoi, E. Ikenaga, D. Gerlach, S. Ueda, Y. Yamashita, T. Chikyow, C. Heske, S. Buecheler, A. N. Tiwari, M. Bär, *ACS Appl. Mater. Interfaces* **2017**, 9, 3581.
- [34] N. Taguchi, S. Tanaka, S. Ishizuka, *Appl. Phys. Lett.* **2018**, 113, 113903.
- [35] P. Schöppe, S. Schönherr, M. Chugh, H. Mirhosseini, P. Jackson, R. Wuerz, M. Ritzer, A. Johannes, G. Martínez-Criado, W. Wisniewski, T. Schwarz, C. T. Plass, M. Hafermann, T. D. Kühne, C. S. Schnorr, C. Ronning, *Nano Energy* **2020**, 71, 104622.
- [36] N. Nicoara, T. Lepetit, L. Arzel, S. Harel, N. Barreau, S. Sadewasser, *Sci. Rep.* **2017**, 7, 41361.
- [37] N. Nicoara, R. Manaligod, P. Jackson, D. Hariskos, W. Witte, G. Sozzi, R. Menozzi, S. Sadewasser, *Nat. Commun.* **2019**, 10, 3980.
- [38] F. Pianezzi, P. Reinhard, A. Chirilă, B. Bissig, S. Nishiwaki, S. Buecheler, A. N. Tiwari, *Phys. Chem. Chem. Phys.* **2014**, 16, 8843.
- [39] I. Khatri, H. Fukai, H. Yamaguchi, M. Sugiyama, T. Nakada, *Sol. Energy Mater. Sol. Cells* **2016**, 155, 280.
- [40] A. Laemmle, R. Wuerz, M. Powalla, *Phys. Status Solidi – Rapid Res. Lett.* **2013**, 7, 631.
- [41] M. Nakamura, K. Yamaguchi, Y. Kimoto, Y. Yasaki, T. Kato, H. Sugimoto, *IEEE J. Photovolt.* **2019**, 9, 1863.
- [42] M. Mezher, L. M. Mansfield, K. Horsley, M. Blum, R. Wieting, L. Weinhardt, K. Ramanathan, C. Heske, *Appl. Phys. Lett.* **2017**, 111, 071601.
- [43] S. Kim, J. Nishinaga, Y. Kamikawa, S. Ishizuka, T. Nagai, T. Koida, H. Tampo, H. Shibata, K. Matsubara, S. Niki, *Jpn. J. Appl. Phys.* **2018**, 57, 055701.
- [44] M. A. Green, *Solid State Electron.* **1981**, 24, 788.

- [45] M. Burgelman, P. Nollet, S. Degraeve, *Thin Solid Films* **2000**, 362, 527.
- [46] S. H. Wei, A. Zunger, *Appl. Phys. Lett.* **1993**, 63, 2549.
- [47] M. Köntges, R. Reineke-Koch, P. Nollet, J. Beier, R. Schaffler, *Thin Solid Films* **2002**, 404, 280.
- [48] R. Scheer, H.-W. Schock, *Chalcogenide Photovoltaics*, Wiley-VCH Verlag, Weinheim, Germany **2011**.
- [49] H. J. Möller, *Semiconductors for Solar Cells*, Artech House, Norwood, MA **1993**, p. 343.
- [50] M. A. Green, *Prog. Photovolt. Res. Appl.* **2009**, 17, 57.
- [51] T. Y. Lin, I. Khatri, J. Matsuura, K. Shudo, W. C. Huang, M. Sugiyama, C. H. Lai, T. Nakada, *Nano Energy* **2020**, 68, 104299.
- [52] T. P. Weiss, S. Nishiwaki, B. Bissig, R. Carron, E. Avancini, J. Löckinger, S. Buecheler, A. N. Tiwari, *Adv. Mater. Interfaces* **2018**, 5, 1701007.
- [53] J. Keller, F. Chalvet, J. Joel, A. Aijaz, T. Kubart, L. Riekehr, M. Edoff, L. Stolt, T. Törndahl, *Prog. Photovolt. Res. Appl.* **2018**, 26, 13.
- [54] D. Abou-Ras, T. Kirchartz, *ACS Appl. Energy Mater.* **2019**, 2, 6127.
- [55] H. J. Leamy, *J. Appl. Phys.* **1982**, 53, R51.
- [56] M. Alt, H. J. Lewenenz, R. Scheer, *J. Appl. Phys.* **1996**, 81, 956.
- [57] Y. Ogawa, A. Jäger-Waldau, T. H. Hua, Y. Hashimoto, K. Ito, *Appl. Surf. Sci.* **1996**, 92, 232.
- [58] R. Würz, W. Hempel, P. Jackson, *J. Appl. Phys.* **2018**, 124, 165305.
- [59] P. Schöppe, S. Schönherr, R. Wuerz, W. Wisniewski, G. Martínez-Criado, M. Ritzer, K. Ritter, C. Ronning, C. S. Schnohr, *Nano Energy* **2017**, 42, 307.
- [60] P. Schöppe, S. Schönherr, P. Jackson, R. Wuerz, W. Wisniewski, M. Ritzer, M. Zapf, A. Johannes, C. S. Schnohr, C. Ronning, *ACS Appl. Mater. Interfaces* **2018**, 10, 40592.
- [61] S. Ishizuka, N. Taguchi, J. Nishinaga, Y. Kamikawa, S. Tanaka, H. Shibata, *J. Phys. Chem. C* **2018**, 122, 3809.
- [62] A. Vilalta-Clemente, M. Raghuvanshi, S. Duguay, C. Castro, E. Cadel, P. Pareige, P. Jackson, R. Wuerz, D. Hariskos, W. Witte, *Appl. Phys. Lett.* **2018**, 112, 103105.
- [63] T. Schwarz, G. Stechmann, B. Gault, O. Cojocar-Mirédin, R. Wuerz, D. Raabe, *Prog. Photovolt. Res. Appl.* **2018**, 26, 196.
- [64] M. Raghuvanshi, A. Vilalta-Clemente, C. Castro, S. Duguay, E. Cadel, P. Jackson, D. Hariskos, W. Witte, P. Pareige, *Nano Energy* **2019**, 60, 103.
- [65] A. Stokes, M. Al-Jassim, A. Norman, D. Diercks, B. Gorman, *Prog. Photovolt. Res. Appl.* **2017**, 25, 764.
- [66] A. Stokes, M. Al-Jassim, D. Diercks, A. Clarke, B. Gorman, *Sci. Rep.* **2017**, 7, 14163.
- [67] C. Persson, A. Zunger, *Phys. Rev. Lett.* **2003**, 91, 266401.
- [68] M. Raghuvanshi, E. Cadel, P. Pareige, S. Duguay, F. Couzinie-Devy, L. Arzel, N. Barreau, *Appl. Phys. Lett.* **2014**, 105, 013902.
- [69] W. Li, Y. Ma, S. Yang, J. Gong, S. Zhang, X. Xiao, *Nano Energy* **2017**, 33, 157.
- [70] C. Persson, A. Zunger, *Appl. Phys. Lett.* **2005**, 87, 211904.
- [71] N. H. Valdes, K. J. Jones, R. L. Opila, W. N. Shafarman, *IEEE J. Photovolt.* **2019**, 9, 1846.